

Ion Thruster Discharge Performance per Magnetic Field Topography

Richard Wirz*, Dan Goebel

Jet Propulsion Laboratory, California Institute of Technology, Pasadena, CA

Conventional DC ion thruster design considers the maximum closed contour to determine favorable mag field configs. Detailed computational analysis shows that important aspects of DC ion thruster performance are determine the magnetic field line, as well as, field strength contours. Primary electrons are highly magnetized and follow field lines. Lower field strengths allow greater ion density since it delays the onset of discharge instability, which leads to a greater performance range. Submitted Abstract – DC-ION is a detailed computational model for predicting the plasma characteristics of rain-cusp ion thrusters. The advanced magnetic field meshing algorithm used by DC-ION allows precise treatment of the secondary electron flow. This capability allows self-consistent estimates of plasma potential that improves the overall consistency of the results of the discharge model described in Reference [refJPC05mod1]. Plasma potential estimates allow the model to predict the onset of plasma instabilities, and important shortcoming of the previous model for optimizing the design of discharge chambers. A magnetic field mesh simplifies the plasma flow calculations, for both the ions and the secondary electrons, and significantly reduces numerical diffusion that can occur with meshes not aligned with the magnetic field. Comparing the results of this model to experimental data shows that the behavior of the primary electrons, and the precise manner of their confinement, dictates the fundamental efficiency of ring-cusp. This correlation is evident in simulations of the conventionally sized NSTAR thruster (30 cm diameter) and the miniature MiXI thruster (3 cm diameter).

Nomenclature

\mathbf{B} = magnetic flux density	J_D = discharge current	$(P_{ps}, P_{pw}, P_{piz}, P_{px}, P_{sw}, P_{siz}, P_{sx}) =$ electron power loss mechanisms (described in text)
$D_{ }$ = parallel plasma diffusion coefficient	J_{DCH} = discharge cathode heater current	r = distance from thruster axis
D_{\perp} = perpendicular plasma diffusion coefficient	J_i = current of ions created in discharge	T_e = secondary electron temperature
D_B = Bohm diffusion coefficient	J_{ip} = current of ions created in discharge by primaries	T_i = ion temperature
f_{inel} = secondary inelastic collision fraction	J_p = primary electron current	T_p = primary electron temperature
f_A = fraction of ion current to anode surfaces	J_{screen} = screen grid ion current	T_o = neutral atom temperature
f_B = fraction of ion current to the beam	\dot{m}_d = discharge chamber propellant mass flow rate	V_{accel} = accelerator grid voltage
f_C = fraction of ion current to cathode surfaces	n_e = secondary electron number density	V_B = beam voltage
F_B = beam flatness	n_i = ion number density (total)	V_D = discharge voltage
J_B = total beam current	n_o = neutral atom number density	V_p = primary electron voltage
J_B^+, J_B^- = beam current and current density due to singly charged ions	n_p = primary electron number density	
J_B^{++}, J_B^{--} = beam current and current density due to doubly charged ions	\dot{n}_e = secondary generation rate density	
	\dot{n}_i = total ion generation rate density	

Greek Symbols

δ_D = plasma magnetization
 δ_V = electron collision ratio

ε_B = discharge loss	$\eta_{ud\{Beam\}}$ = discharge propellant utilization efficiency per Ion Diffusion Sub-Model	ζ_o = grid transparency to neutral atoms
γ_{nc} = non-classical collision parameter		ζ_i = grid transparency to ions
Γ = particle flux	η_{ud} = discharge propellant utilization efficiency	
Γ_e = electron flux		
$\eta_{ud\{Gas\}}$ = discharge propellant utilization efficiency per Neutral Atom Sub-Model	ν_{e-o} = neutral-centered electron collision frequency	
	ν_{e-i} = ion-centered electron collision frequency	

Units:

This study uses mks units of the International System (SI) with the exception that energies are frequently given in terms of electron volts (eV).

sccm \equiv Standard Cubic Centimeters per Minute. For xenon: 1 sccm \approx 0.09839 mg/s at STP.

eV/ion \equiv (Watts of Discharge Power)/(Amp of Beam Current) for discharge loss, ε_B

I. Introduction

A. Background and Motivation

DC Ring-Cusp Ion Thruster Discharges

For DC ion thrusters, the power needed to ionize the neutral propellant atoms comes from high-energy electrons that are emitted from the discharge cathode. These primary electrons (or “primaries”) are accelerated to relatively high energies by the (~25V) discharge voltage applied between the cathode and anode surfaces. A magnetic field is used to prevent the loss of electrons to the anode surface to increase ionization efficiency. For a ring-cusp discharge, as shown in Figure figionthruster, alternating rings of high-strength magnets (typically SmCo) are used to provide magnetic confinement of the primaries at the magnetic cusps and throughout the discharge volume. For a typical ring-cusp thruster, the magnets are arranged so that the magnetic field lines primarily terminate on cathode potential surfaces or at cusps on the anode surfaces. In this way, primaries are confined by magnetic reflection at the cusps or by electrostatic forces at the cathode potential surfaces. The magnetic cusps are placed at anode surfaces to allow lower energy electrons (“secondaries”) to be lost along the field lines to carry the discharge current and maintain discharge stability [refTh15]. The low-energy secondaries are produced by primary electron collisions with plasma species and ionization by other secondaries.

Neutral propellant atoms are injected into the discharge chamber through a main propellant feed, the location of which varies from thruster to thruster. Most conventional DC thrusters use a hollow cathode, which requires propellant to run, so additional propellant is introduced through the hollow cathode orifice. At this time, the most widely used propellant is xenon due mainly to its high mass, low-risk handling, and relatively high second ionization threshold; however, other propellants may be used [refTh3].

Discharge Performance and Stability

DC ring-cusp ion thruster discharge performance is dominated by two competing parameters: plasma confinement efficiency and discharge stability. Plasma confinement efficiency requires sufficiently strong magnetic fields to confine the plasma (including primaries) at the cusps and throughout the bulk of the plasma. Magnetic confinement of the bulk plasma is conventionally thought of as “closing” a certain B-field contour, typically on the order of 10s of Gauss as discussed in Beattie [refTh17]. This concept is assumed to assure that the plasma is reasonably confined between the cusps. For larger diameter ring-cusp ion thrusters, such as NEXIS (~60cm) and NEXT (~40cm), additional magnetic rings were added to close a sufficiently high B-field contour for desirable plasma confinement [refTh18].

Conventional parameters for assessing discharge performance for DC ion thrusters include:

- f_B – percentage of ions extracted to the beam
- ε_B – beam ion energy cost
- C_o – primary electron utilization

Complete descriptions of these parameters are provided by Reference [RefBrophy].

Another important discharge performance parameter is the discharge propellant utilization, η_{ud} (the fraction of the discharge propellant flow that leaves the thruster as beam ions), which is calculated by

$$\eta_{ud} \equiv \frac{(J_B^+ + J_B^{++}/2)m_i}{em_d} \quad \text{[Eq Th2.2-5]}$$

where \dot{m}_d and m_i are the mass flow rate of discharge propellant and the ion mass, e is electron charge, and J_B^+ and J_B^{++} are the beam currents due to single and double ions, respectively. In other references, this is sometimes referred to as $\eta_{ud[corr]}$, which stands for “propellant utilization corrected” since it corrects the misleading conventional measurements that do not account for double ion content.

Discharge stability for ring-cusp ion thrusters can be understood by examining the behavior of the plasma near the cusps. Many detailed experiments and models have been used to explain the behavior of the plasma in the cusp region [refTh19, refTh20, refTh15, refTh21, refTh22]. Leung, et al [refTh19] showed that primary electrons are typically very well confined at the cusp and that plasma losses to the cusps may be described using a hybrid ion-electron gyroradius. This parameter was used by Goebel [refTh15] to explain the discharge instabilities that can result for cusp magnetic field strengths that are too high for certain plasma conditions. These discharge instabilities are due to overly high cusp B-field strengths that can cause an electron current continuity imbalance that leads to plasma discharge loss due to impedance shift instabilities. The continuity imbalance arises from the reduction in plasma loss area that results from increased cusp strengths, as observed by Leung and Hershkowitz [refTh19, refTh20]. If the cusp B-field is too strong then the plasma potential, which is normally positive, will tend negative to satisfy current continuity for a particular range of electron production rates in a cusp confined plasma. This lower plasma potential reduces the energy of the primary electrons emitted from the cathode, leading to a runaway of the plasma potential indicative of an unstable discharge. The discharge instabilities impose an upper-limit for the cusp B-field for a given plasma conditions, as observed at certain operating conditions for ion thrusters.

Beam Flatness, (Grid Performance and Utilization)

The purpose of the discharge chamber is to efficiently provide ions for extraction through the grids, while the grids prevent the loss of propellant neutrals and allow ions to be extracted and accelerated. The degree to which the discharge provides favorable plasma conditions to the region immediately upstream of the grids can be determined by examining the beam and neutral loss profiles at the grid exit plane. To assess how evenly the ion extraction grids are being used, the beam flatness parameter, F_B , relates the average to the peak beam current density by

$$F_B = \frac{\int_0^R 2\pi r j_B(r) dr}{\pi R^2 j_{B\max}} \quad \text{[EqTh2.2-18]}$$

where r , R , j_B , and $j_{B\max}$ are the radial coordinate of the beam, the total grid radius, and local and maximum beam current density [refTh13]. To understand the full impact of beam flatness on thruster throttleability it is helpful to use a beam flatness based on the number of ions, instead of the charge of ions, since this is more representative of the absolute ion density upstream of the grids. This viewpoint for beam flatness is useful since double ions tend along single ion trajectory paths. Therefore, for a beam flatness based on the ion flux ions of all charges we use

$$F_{B^*} = \frac{\int_0^R 2\pi r \left[j_B^+(r) + \frac{1}{2} j_B^{++}(r) \right] dr}{\pi R^2 \left[j_{B,\max}^+ + \frac{1}{2} j_{B,\max}^{++} \right]} \quad \text{[EqTh2.2-18]}$$

where $j_{B,\max}^+$ and $j_{B,\max}^{++}$ are assumed to occur at the same radial location on the grids.

As discussed in many references [refTh14, refTh7], a high flatness parameter typically reflects favorable grid utilization, high throttleability, and maximum grid life. Since the beam flatness is directly related to the plasma distribution in the discharge chamber, a low flatness parameter, even though it manifests in low “grid” life and performance, is more appropriately attributed to poor discharge design.

Performance Effects due to Double Ion Content

Double ions typically hurt thruster performance since they require nearly twice the electron energy to create as single ions, accelerate wear mechanisms, and deliver reduced thruster per unit of ion current. For example, the double ion thrust correction factor is defined as

$$\alpha = \left(1 + \frac{J_B^{++} \sqrt{2}}{J_B^+ 2}\right) / \left(1 + \frac{J_B^{++}}{J_B^+}\right) \quad [\text{EqTh2.2-11}]$$

Discharge chambers should be designed to minimize double ionization to avoid the performance losses. Measurements of conventional ion thruster beams show a noticeable (>8%) fraction of double ions [refTh16]; thus showing that state-of-the-art thruster design may be improved by reducing this phenomenon.

Discharge Plasma Magnetization

For the computational model (DC-ION) used in this analysis, the ratio of the parallel and perpendicular plasma diffusion coefficients is used to quantify the “magnetization,” δ_D , of the plasma motion in different regions of the thruster by

$$\delta_D = D_{\parallel} / D_{\perp} \quad [4.5-60]$$

The derivation and definitions of D_{\parallel} and D_{\perp} are given in Reference [RefJPC05mod1]

B. Objective

In this study, we employ JPL’s Ion Thruster Model (DC-ION) to investigate the relationship of magnetic field lines and contours on discharge performance by comparing the performance and discharge characteristics of various modifications to the NSTAR magnetic field.

II. General Approach

A. Comparing Discharge Chamber Magnetic Field Lines and Contours for 3-ring NSTAR Configurations

The maximum closed contour for the baseline NSTAR magnetic field is 27 Gauss, as shown in Figure figbaseline. This design (referred herein as “Config 1”) is sufficient to achieve the impressive performance of the NSTAR thruster; however, an unfortunate aspect of the baseline NSTAR design is the large region of magnetic field lines that run parallel to the thruster axis. These axially-oriented magnetic field lines starting at the cathode exit and terminating at the grids cause “over-confinement” of the primary electrons on axis, which leads to the very large double ion peak observed in NSTAR beam profiles [refWirzJPC05].

In this study we take the NSTAR baseline and alter it to separately and collectively examine the effects of changing magnetic field lines and/or contours.

Increased NSTAR performance and a more favorable beam profile is achieved by simply strengthening the mid-magnet ring, as shown in Figures figmod1 and figcompare1.

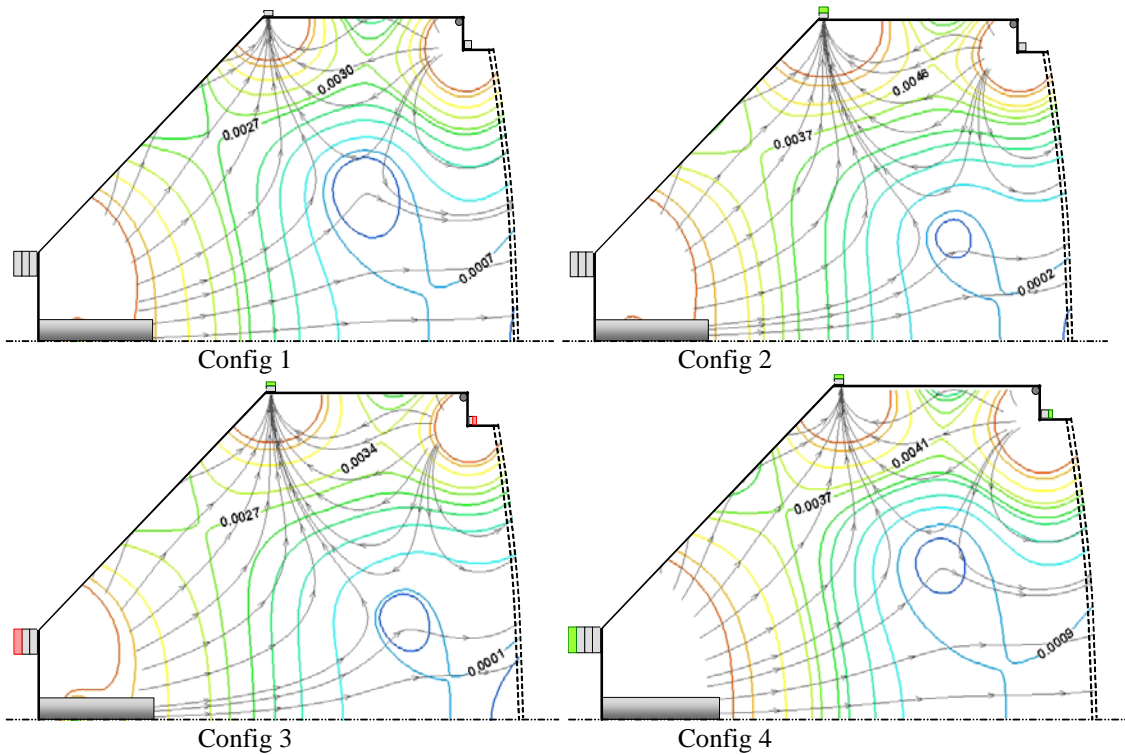


Figure figconfigs. NSTAR magnetic field configurations:
 Config 1 is the NSTAR baseline. Config 2 is NSTAR with double-strength mid magnet ring.
 Config 3 has identical field lines to Config 2 but with weaker magnets to simulate baseline (Config 1) field strength.
 Config 4 has identical field lines to Config 1, but with stronger magnets to simulate Config 2 field strength.
 Additions to baseline magnet sizes are shown in green, reductions are shown in red.

By comparing Figures figbaseline and figmod1, we see that the improved NSTAR configuration (referred herein as “Config 2”) exhibits an increased maximum closed contour (37 Gauss) and a significant reduction of axially-oriented magnetic fields lines. To separately investigate the relative importance of these two improvements, we introduce two new NSTAR configurations:

- Config 3, shown in Figure FigConfig3 - The first of the new configurations (“Config 3”) maintains the exact magnetic field line topography of Config 2 (improved NSTAR) but the overall magnetic field strength is reduced to close the 27 Gauss contour as in baseline NSTAR (Config 1). This configuration is achieved by simply proportionally reducing the depth along the magnetization direction (and hence the magnetic dipole moment) of all magnets from Config 2.
- Config 4, shown in Figure figconfig4 - In a similar fashion, we generate Config 4 to maintain the B-field line topography of the NSTAR baseline (Config 1) but with an increased magnetic field strength sufficient to close the 37 Gauss contour as in Config 2.

Compare:

- 1 and 3 – effect of changing field structure of baseline
- 1 and 4 – effect of uniformly increasing the field strength of NSTAR baseline
- 1 and 2 – changing both field lines and contour
- 2 and 3 – increasing field strength of an already favorable field line structure

B. Comparing 3-ring and 4-ring NSTAR geometries

The effect of the number of magnetic rings is shown by simply adding another ring to the baseline NSTAR thruster. We also increase and decrease the 4-ring magnet strength to show the effects on performance.

C. Computational Model and Experimental Reference

JPL's Ion Thruster Model (DC-ION) has been validated against performance and beam profile data for the NSTAR and MiXI thrusters. Reference [RefWirzJPc05] introduced DC-ION (referred to as DCM at the time) in its present form and presented the validation of DC-ION against NSTAR data at multiple operating conditions and power levels. Reference [RefWirzJPc05] also presented the analysis where DC-ION predicted the performance benefits of the improved NSTAR configuration (Config 2), which were validated by subsequent experimental measurements.

The thruster inputs and assumptions used by DC-ION for this study are identical to those in Reference [RefWirzJPc05].

III. Results

A. Comparison of Discharge Performance

Discharge Performance Parameters

The results of the model are expressed by averaged discharge performance parameters at the Micro-Ion mTH1 operating condition and are compared to the thruster data in Table tabresults. Variable definitions are given in the nomenclature list. The agreement of η_{ud} and ε_B is a consequence of the choice of throttle point. Comparing J_i and J_{ip} shows that the primary electrons are responsible for ion generation in the Micro-Ion thruster. The parameters in Table tabresults are defined as follows:

η_{ud} – discharge propellant efficiency defined in Equation Eq Th2.2-5

ε_B – discharge loss [eV/ion]

$J_{B^{++}}/J_{B^+}$ - ratio of beam current due to doubly- and singly charged ions

J_i – current of ions created in discharge [A]

J_{ip} – current of ions created in discharge by primaries [A]

n_i – average density of ions [m^{-3}]

n_p – average density of primary electrons [m^{-3}]

n_o – average density of neutrals [m^{-3}]

f_A – fraction of ion current to anode surfaces

f_B – fraction of ion current to the beam

f_C – fraction of ion current to cathode surfaces

F_B – beam flatness as defined by jB [++] profile

F_{B^*} – beam flatness as defined by jB [+] profile

The results in Table 1 show the relative performance of the configurations. For figure figdisparams consolidates key discharge parameters for all configurations.

Table 5.2-1. Discharge Performance Parameters
(NSTAR - TH15 Simulation vs. Data)

Discharge Parameters	η_{ud}	ϵ_B	$J_{B^{++}}/J_{B^+}$	J_i	J_{ip}	n_i	n_p	n_o	f_A	f_B	F_B	F_{B^*}
Units	%	eV/ion	-	mA	mA	m^{-3}	m^{-3}	m^{-3}	-	-	-	-
Config 1 NSTAR baseline	85.6	187	0.129	6.1	3.73	$1.97 \cdot 10^{17}$	$9.25 \cdot 10^{15}$	$4.64 \cdot 10^{18}$	0.66	0.29	0.47	0.67
Config 2	90.6	181	0.083	6.7	3.62	$1.79 \cdot 10^{17}$	$1.02 \cdot 10^{16}$	$3.70 \cdot 10^{18}$	0.62	0.33	0.68	0.71
Config 3	87.6	189	0.062	6.7	3.94	$1.88 \cdot 10^{17}$	$7.95 \cdot 10^{15}$	$4.41 \cdot 10^{18}$	0.64	0.30	0.72	0.74
Config 4	88.8	177	0.182	6.5	3.53	$1.84 \cdot 10^{17}$	$1.74 \cdot 10^{16}$	$3.71 \cdot 10^{18}$	0.63	0.32	0.29	0.48
Config 5	90.6	181	0.083	6.7	3.62	$1.79 \cdot 10^{17}$	$1.02 \cdot 10^{16}$	$3.70 \cdot 10^{18}$	0.62	0.33	0.68	0.71

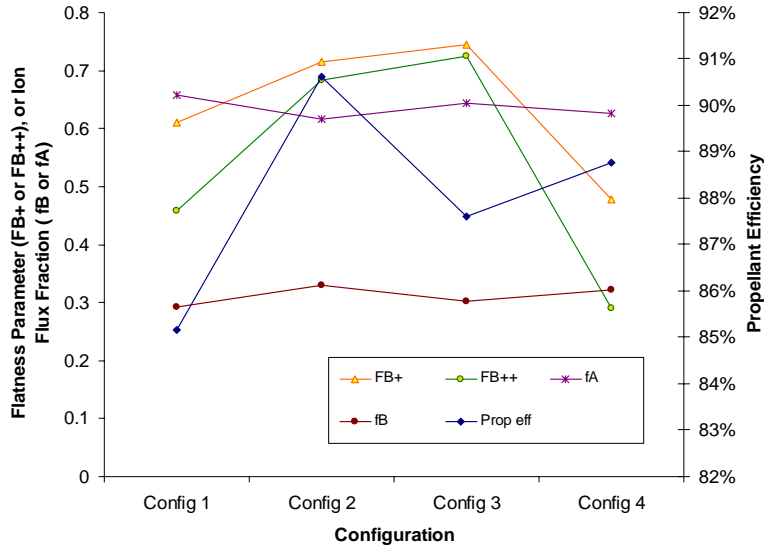
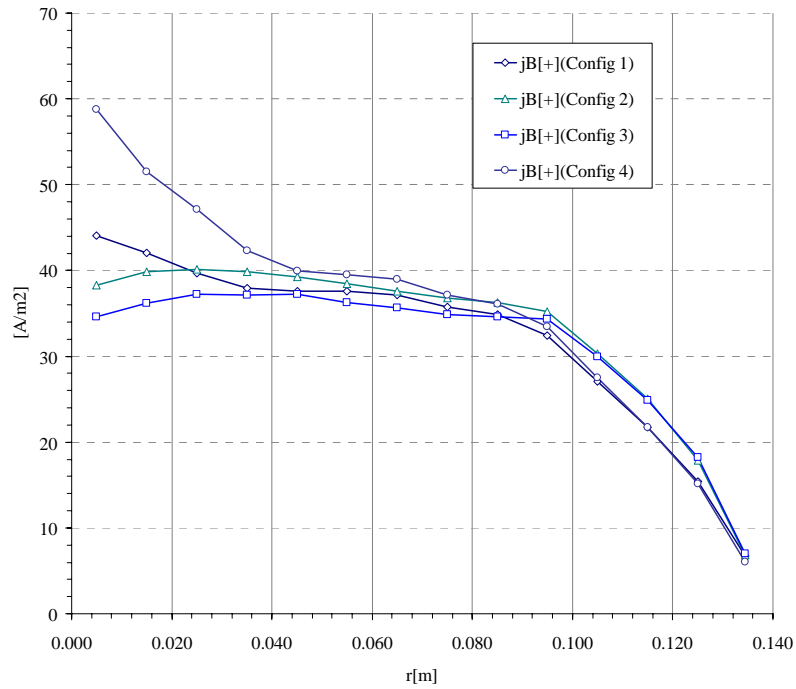
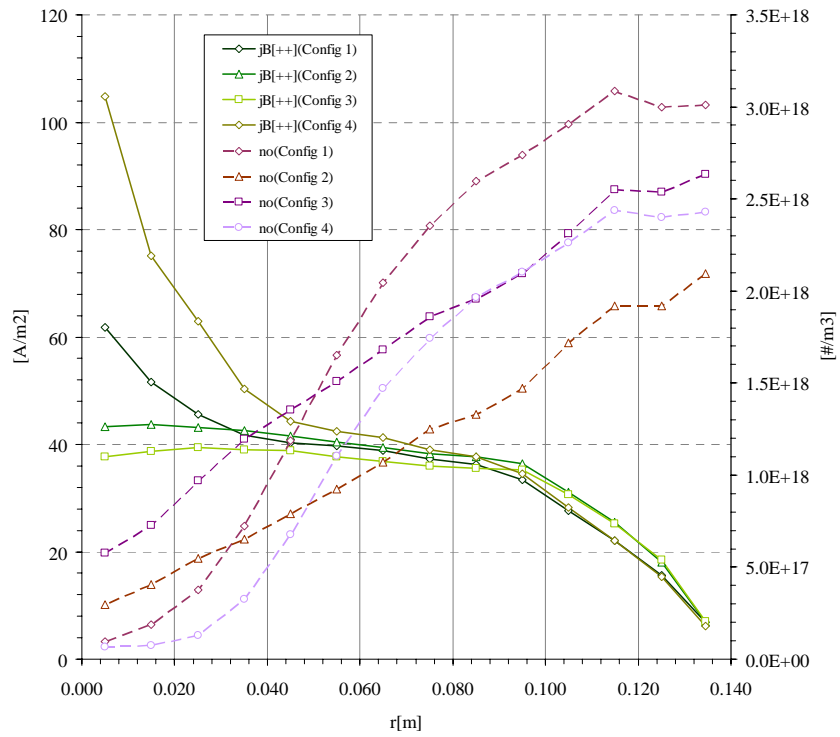


Figure figdisparams. Important discharge parameters for the NSTAR configurations

The beam current density profiles along the dished exit plane of the thruster, as calculated by DC-ION, are shown in Figures figjB+profile and figjB++profile. In these figures, $jB[+]$ assumes that all beam ions are singly charged (i.e., $jB[+] = [j_B^+ + j_B^{++}/2]$), while $jB[++]$ includes doubly charged ion effects (i.e., $jB[++] = j_B^+ + j_B^{++}$). The variables j_B^+ and j_B^{++} are the single ion and double ion current densities, respectively. Comparing these profiles shows the radially dependent effect of double ions on measured beam current. The neutral densities (just upstream of the grids) show that the more peaked profiles correlate with a larger gradient in neutral density across the grids.



Figj+profile. Beam profiles for jB[+] for all configurations.



Figj++profile. Beam profiles for jB[++] and neutral density profiles for all configurations.

Two-Dimensional Plots of Discharge Characteristics

Figure figmagz shows the variation of “magnetization,” δ_D , of the plasma motion for the different thruster configurations.

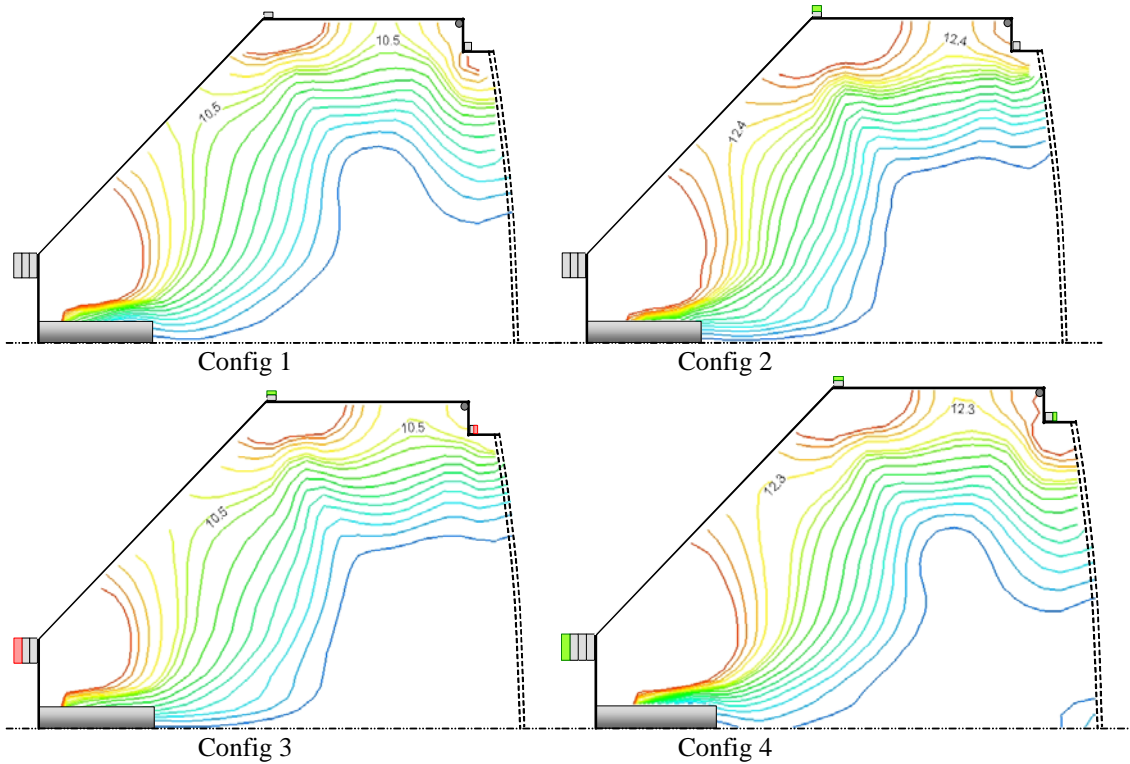


Figure figmagz. Magnetization, δ_D , for the different thruster configurations. Additions to baseline magnet sizes are shown in green, reductions are shown in red.

C. Multi-Ring Field Topography

3-, 4-, 5-, and 6-ring configurations.

IV. Discussion and Conclusions

The results from this investigation show that the magnetic field lines dictate the paths of the high-energy primary electrons. It is important to design the magnetic field structure to deliver the primaries efficiently throughout the useful volume of the thruster, especially that just upstream of the ion extraction grids. To assure that the primaries are not trapped along the thruster axis it is desirable to locate the minimum B-field point as close to the axis as possible for discharges with an odd number of rings, such as a 3-ring discharge. Discharges utilizing an even number of magnetic rings, such as a 4-ring, inherently place a magnetic minimum on-axis, which encourages the primary electrons to move throughout the discharge chamber. Herein we confirm that the magnetic confinement of the plasma is proportional to the maximum closed field line; however, it is important that a stronger magnetic field does not cause severe confinement of the plasma to the point that a high percentage of double ions are created.

Acknowledgments

The research described in this paper was carried out by the Jet Propulsion Laboratory, California Institute of Technology, under a contract with the National Aeronautics and Space Administration in support of Project Prometheus.

References

- [refJPC05mixi1] – Wirz R., “Discharge Plasma Processes of Ring-Cusp Ion Thrusters,” Ph.D. Dissertation, Aeronautics, Caltech, Pasadena, CA, 2005
- [refJPC05mixi2] – Wirz R., Polk J., Marrese C., Mueller J., “Development and Testing of a 3cm Electron Bombardment Micro-Ion Thruster,” IEPC Paper 01-343, 27th IEPC, Pasadena, CA, Oct 2001
- [refJPC05mixi3] – Wirz R., Polk J., Marrese C., Mueller J., “Experimental and Computational Investigation of the Performance of a Micro-Ion Thruster,” AIAA-2002-3835, 38th JPC, Indianapolis, IN, July 2002
- [refJPC05mixi4] – Wirz R., Mueller J., Gale M., Marrese C., “Miniature Ion Engine for Precision Formation Flying,” AIAA-2004-4115, 40th Joint Propulsion Conference, Ft. Lauderdale, FL, 2004
- [refJPC05mixi5] – Wirz R., Katz I., “Plasma Processes of DC Ion Thruster Discharge Chambers,” AIAA Paper 2005-3690, 41st AIAA Joint Propulsion Conference, Tucson, AZ, 2005.
- [refJPC05mod1] - Wirz R., Katz I., “Plasma Processes of DC Ion Thruster Discharge Chambers,” 41st JPC, Tucson, AZ, July 2005